

# Evolution of the 0.01 – 25 Hz power spectral components in Cygnus X-1

Magnus Axelsson, Luis Borgonovo, and Stefan Larsson

Stockholm Observatory, AlbaNova, SE- 106 91 Stockholm, Sweden

Received 12 November 2004/ Accepted 2 April 2005

**Abstract.** Analyzing the archival data from the *Rossi X-ray Timing Explorer* (RXTE), we study the power density spectra (PDS) of Cygnus X-1 from 1996 to 2003 in the frequency range of 0.01 – 25 Hz. Using a model consisting of one or two Lorentzians and/or an exponentially cut-off power-law, we are able to achieve a good fit to the PDS during the observations. With our model we are also able to track the evolution of the Lorentzian components through all spectral states of the source. We confirm the relation between characteristic frequencies seen both in black hole candidate and neutron star sources, and show the changes in this relation during the transitional and soft states of the source. The connection between the Lorentzian components is investigated by analyzing similarities and differences in their behavior. We find that the spectral state of the source can be uniquely determined from the parameters of these components. The parameter correlations can all be described by continuous functions, which differ between components. We discuss our results in the context of relativistic precession model for the accretion disk, and show a remarkable agreement between the model prediction and the data in the hard state. We estimate a value for the specific angular momentum of  $a_* = 0.49$  ( $-0.57$ ) in the case of prograde (retrograde) rotation and an estimate for the inner radius of 22 to 50 (25 to 55) gravitational radii. Additional assumptions are required to explain the soft state data, and attempting to invoke rotational reversal for state transitions shows that it is insufficient to explain the differences between the hard and soft state data.

**Key words.** Stars: individual: Cyg X-1 – X-rays: binaries – Accretion, accretion disks

## 1. Introduction

In many X-ray binary systems, the existence of distinct spectral states has been well documented. Often quoted as a prototype black hole system, Cygnus X-1 has been extensively observed and modeled. The source exhibits two main spectral states, usually referred to as hard and soft, with a brief intermediate state (sometimes interpreted also as a very high state, see e.g. discussion in Zdziarski & Gierliński 2004, and references therein) during the transitions. Several models have been proposed to explain the spectral states and transitions, with the two main components being a geometrically thin, optically thick accretion disk and a hot inner flow or corona. Seed photons from the disk are believed to gain energy in the corona through Comptonization (Shapiro et al. 1976). The models vary in the geometry and properties of mainly the corona/comptonizing region (for a review on coronal models, especially in regard to timing characteristics, see Poutanen 2001). However, changes in the inner radius of the accretion disk are a common source of variability in many models (e.g. Poutanen et al. 1997; Esin et al. 1998; Churazov et al. 2001; Zdziarski et al. 2002).

The changes in spectral state are evident also in the power density spectrum (PDS). In the hard state the PDS is characterized by a flat-topped component up to  $\sim 0.2$  Hz, where it breaks to a  $f^{-1}$  slope that steepens at a few Hz (e.g. Belloni & Hasinger 1990; Nowak et al. 1999). In the soft state the PDS is dominated by a  $f^{-1}$  component that steepens around 10 Hz (e.g. Cui et al. 1997a). The 1996 state transition also revealed an intermediate PDS, showing a  $\sim f^{-1}$  slope at lower frequencies, a flatter component around 0.3 – 3 Hz, and above that similar to the hard state PDS. In many observations there is evidence for a quasi-periodic oscillation (QPO) at a few Hz (Belloni et al. 1996; Cui et al. 1997b; Cui 1999).

Previous studies of the PDS of Cyg X-1 have shown correlations between temporal and spectral components (e.g. Gilfanov et al. 1999) and also between different temporal features. Correlations between features in the hard state PDS were first reported by Wijnands & van der Klis (1999). To resolve the origin of the temporal features, it is vital to understand their long term behavior. Pottschmidt et al. (2003, hereafter P03) recently presented a large scale study of the hard state PDS and also included data from ‘failed state transitions’. However, no study has been presented where the PDS for all spectral states of Cyg X-1 are consistently modeled. To this end, we conducted a systematic analysis of all the available data from the *Rossi X-Ray Timing Explorer* (RXTE) satellite observations

Send offprint requests to: M. Axelsson,  
e-mail: magnusa@astro.su.se

of Cyg X-1 in the HEASARC public archives. Using a model consisting of a power-law and two Lorentzian profiles, we were able to fit the majority of PDS, and to follow the components from hard state through the transitions and back. This allowed us to expand on previous results and monitor the evolution of the components.

Our aim in this paper is to provide a consistent description of the PDS of Cyg X-1 in all states, and through this study the evolution of the PDS throughout the time it has been observed by RXTE. We begin with a brief description of the available data, the computation of lightcurves and power spectra, and a presentation of our models in Sect. 2. This is followed by a presentation of our results, where we show the behavior of the different model components (Sect. 3). In Sect. 4 we follow with a discussion of the components, as well as putting our results in the context of physical models. Finally we summarize our findings in Sect. 5.

## 2. Observations and Data Analysis

### 2.1. The archival data

Since its launch on December 30, 1995, and until the end of April 2004, the RXTE satellite has observed Cyg X-1 in more than 750 pointed observations. The satellite has an orbital period of about 5.8 ks, but due to its low circular orbit, typical on-source time in a pointed observation is 3 – 4 ks. The satellite also carries an All-Sky Monitor (ASM) instrument on board, which continuously scans the sky, covering 80% every orbit.

In this study we have used all public pointed observations, with data from the Proportional Counter Array (PCA, Jahoda et al. 1996). The PCA consists of five identical Proportional Counter Units (PCUs), and is sensitive in the 2-60 keV energy range. The observations span the time from January 8, 1996 to April 3, 2004. The data mode used was the ‘Generic Binned’ mode.<sup>1</sup> For the count (hardness) ratios (see Sect. 2.4) we used data in the Standard2 configuration. Due to the different configurations and epochs for the observations, it was not always possible to obtain an exact match between energy ranges. We found that choosing the energy range of  $\sim 2 - 9$  keV allowed us to maintain the same range fairly well throughout the observations, with any deviations appearing in the upper boundary. We note that the shape of the PDS of Cyg X-1 is not very sensitive to the width of the energy band in this region (Nowak et al. 1999; P03), so the slight variations in the upper boundary should not affect our results. For the hardness ratios, the use of Standard2 data enabled us to keep the same energy ranges throughout the epochs. The channels and corresponding energy ranges are presented in Table 1.

We used the standard RXTE analysis software FTOOLS, Version 5.2. Lightcurves and X-ray spectra were extracted using standard screening criteria: a source elevation  $> 10^\circ$ , a pointing offset  $< 0.01$  and a South Atlantic Anomaly exclusion time of 30 minutes. For the PDS, the lightcurves were extracted with a time resolution of 10 ms (for a few observations a time resolution of 16 ms was the highest possible, due to

**Table 1.** Channel and energy ranges used in the count ratios and PDS.

	Count ratios		PDS
	Lower band	Upper band	Upper channel <sup>a</sup>
PCA Epoch 1			
channel	0 – 10	30 – 60	35
energy (keV)	$\sim 2 - 4$	$\sim 9 - 20$	9.5
PCA Epoch 2			
channel	0 – 6	25 – 54	29
energy (keV)	$\sim 2 - 4$	$\sim 9 - 20$	9.3
PCA Epoch 3			
channel	0 – 6	21 – 50	21 – 26
energy (keV)	$\sim 2 - 4$	$\sim 9 - 20$	8.0 – 9.8
PCA Epoch 4			
channel	0 – 5	16 – 42	20 – 22
energy (keV)	$\sim 2 - 4$	$\sim 9 - 20$	8.8 – 9.7
PCA Epoch 5			
channel	0 – 5	17 – 44	21 – 22
energy (keV)	$\sim 2 - 4$	$\sim 9 - 20$	9.3 – 9.7

<sup>a</sup> Only the upper channel and energy boundaries are given, the lower boundary is  $\sim 2$  keV in all datasets. For epochs 3 to 5, the upper boundary varied according with the channel binning used in the observation, and the ranges of upper channels and corresponding energies are given.

the available data mode). The lightcurves used in determining count ratios were extracted with 16 s time resolution. To allow comparison between observations during different epochs and using different numbers of PCUs, the lightcurves were all normalized to one PCU.

The data taken from the ASM instrument are the one-day average count rates. All three bands have been combined, and the energy range is  $\sim 2 - 12$  keV.

### 2.2. Calculating the power density spectra

To calculate the power density spectra the high-resolution light curves were divided into segments of  $2^{13}$  bins ( $\sim 82$  s) and a Fourier transform performed on each segment. The resulting PDS were then gathered into groups of 10 and each group averaged into one final PDS. Unfortunately, calculating the PDS over short segments results in a low frequency resolution and we were therefore not able to model any narrow features in the PDS. Reducing the number of averaged segments increases the statistical fluctuations. However, our approach allows changes in the PDS on timescales as short as  $\sim 15$  minutes to be monitored. Our preliminary studies showed that such changes do in fact occur, and as a result we accepted the lower signal-to-noise ratio. This is further discussed in Sect. 3.1.

The frequency range in our observations is 0.01-25 Hz. The PDS are corrected for the Poisson level. In principle, dead-time effects should be considered when determining the Poisson level. For the frequency range used here this correction is very small ( $\lesssim 2\%$ ) compared to the statistical fluctuations, and we therefore disregard it. As the effect of deadtime increases with frequency, we set our upper limit to 25 Hz. For a discussion

<sup>1</sup> For one observation run in epoch 1, P10240, only data from the single-bit mode was available, with the energy range  $\sim 2 - 9.5$  keV.

on dead-time influence on PDS see Vikhlinin et al. (1994) and Zhang et al. (1995), and for its relevance in the case of the PCA detector Zhang et al. (1996) and Jernigan et al. (2000).

The PDS normalization used in this paper is that of Belloni & Hasinger (1990) and Miyamoto et al. (1992). In this normalization, integrating over a frequency range gives the square of the fractional root mean square (RMS) variability in that frequency interval. The PDS are shown both in units of power versus frequency and frequency times power versus frequency ( $fP_f$  versus  $f$ , see e.g. Belloni et al. 1997). The latter method of presenting the PDS more clearly shows the contribution of variations per frequency decade to the total RMS of the source. The PDS have been rebinned to semi-logarithmically spaced bins.

The observations were provisionally divided into groups, roughly depending on the state of the source. Figure 1 shows the ASM lightcurve of Cyg X-1, and the vertical lines show boundaries between the different groups. The intervals around the transitions are deliberately chosen wide in order to encompass hard and soft state PDS before and after each transition. A period of intense flaring activity in the hard state (and possibly one or more brief transitions to the soft state during MJD 51 830 – MJD 51 960, see Cui et al. 2002) was treated separately. The reduction resulted in a total of 2016 PDS, of which 1324 were from the hard state, 226 in flares, 191 during transitions, and 275 in the soft state. Approximately 2% of the computed PDS were of too low quality to be used in the analysis.

### 2.3. Modeling

The PDS of Cyg X-1 have traditionally been described using a double-broken power-law in the hard state (e.g. Belloni & Hasinger 1990; Nowak et al. 1999) and an  $f^{-1}$  slope broken at higher frequencies in the soft state (Cui et al. 1997a; Cui 1999; Churazov et al. 2001). Building on results from comparisons between neutron star (NS) and black hole candidate (BHC) sources (Psaltis et al. 1999; Wijnands & van der Klis 1999, and references therein) it has been shown that models using Lorentzian profiles provide a good description of the hard state of Cyg X-1 (Nowak 2000, hereafter N00; P03). However, these models do not fit the soft state of Cyg X-1, and during large flares and state transitions an additional power-law component is required (P03).

While there is evidence for several Lorentzian profiles in the PDS of Cyg X-1, generally only two dominate at a given time (N00; Gilfanov et al. 1999). As a base for our model we therefore consider the sum of two Lorentzian profiles of the form

$$L_i(f) = \frac{H_i W_i v_i}{(f - v_i)^2 + f W_i v_i} \quad (1)$$

where  $H_i$  is the value of  $fP_f$  at the peak frequency  $v_i$ . In the  $fP_f$  representation, the dimensionless parameter  $W_i$  gives a measure of the width of the profile. The parametrization is chosen such that for a given  $W_i$  and  $H_i$ , the integral of the Lorentzian (and thus its fractional contribution to the total RMS variability) is the same for any value of  $v_i$ . Note that while this parametrization differs from others previously used (e.g. N00;

**Table 2.** Combinations of components used.

Model	Components	States used
1	2 Lorentzians	hard
2	Power-law+2 Lorentzians	all
3	Power-law+Lorentzian	soft
4	Power-law	soft

P03), it has the advantage of having a direct interpretation of the parameters in the  $fP_f$  representation.

We have chosen to use the peak frequency, which is the frequency where the contribution of the Lorentzian to the total RMS is at its maximum, rather than the centroid frequency, since this seems to be the important parameter in terms of frequency relations (N00; van Straaten et al. 2002). In the case of narrow features, the peak and centroid frequencies will be virtually identical. For broad features (such as breaks in the standard PDS representation), it is the peak frequency which best represents the characteristic frequency of the feature. In such cases the centroid frequency has no direct physical meaning, and will approach zero. For further discussion on the peak and centroid frequencies see Belloni et al. (2002).

The fitting is done in the  $fP_f$  parameter space, where our parameters have the interpretation described above. Conversion to ‘standard’ Lorentzian parameters shows the advantage of using the peak frequency. When the width parameter  $W_i$  is greater than 2, the centroid frequency for the Lorentzian in the PDS space becomes negative. Although not a problem mathematically, this underscores the fact that in the context of broad components it is the peak frequency that has a physical interpretation. In principle we could have frozen the centroid frequency to zero in such cases, but we left it free in order to better follow the variations of the PDS at very low frequencies.

In addition to the Lorentzian profiles, when necessary (large flares, transitions and in the soft state) we have included a cut-off power-law component of the form

$$P(f) = A f^{-\alpha} e^{-f/f_c} \quad (2)$$

where  $A$  is the normalization constant,  $\alpha$  is the power-law index, and  $f_c$  is the turnover frequency. Studies at longer timescales of Cyg X-1 using RXTE/ASM data (Reig et al. 2002) show that at low frequencies (below  $\sim 10^{-5}$  Hz) the PDS is approximately described by a  $\sim f^{-1}$  power-law, and there is evidence that the PDS follows this index to higher frequencies during transitions and in the soft state (Zdziarski et al. 2004). A simple  $f^{-1}$  power-law does not fit the soft state PDS above  $\sim 10$  Hz, and we therefore introduce an exponential cut-off.

As will be described in Sect. 3, when the second Lorentzian shifts to higher frequencies in the soft state, its contribution diminishes and it becomes difficult to constrain. Some PDS were therefore fit with only one Lorentzian profile plus a power-law component. In addition, the canonical soft state PDS exhibiting only a  $f^{-1}$  slope do not require any Lorentzian profile. Table 2 lists the component combinations used in each state, and example fits for each of the four models are shown in Figs. 2 to 6.

While it is clear that Cyg X-1 exhibits several spectral states, there is no unique classification between them. Adding

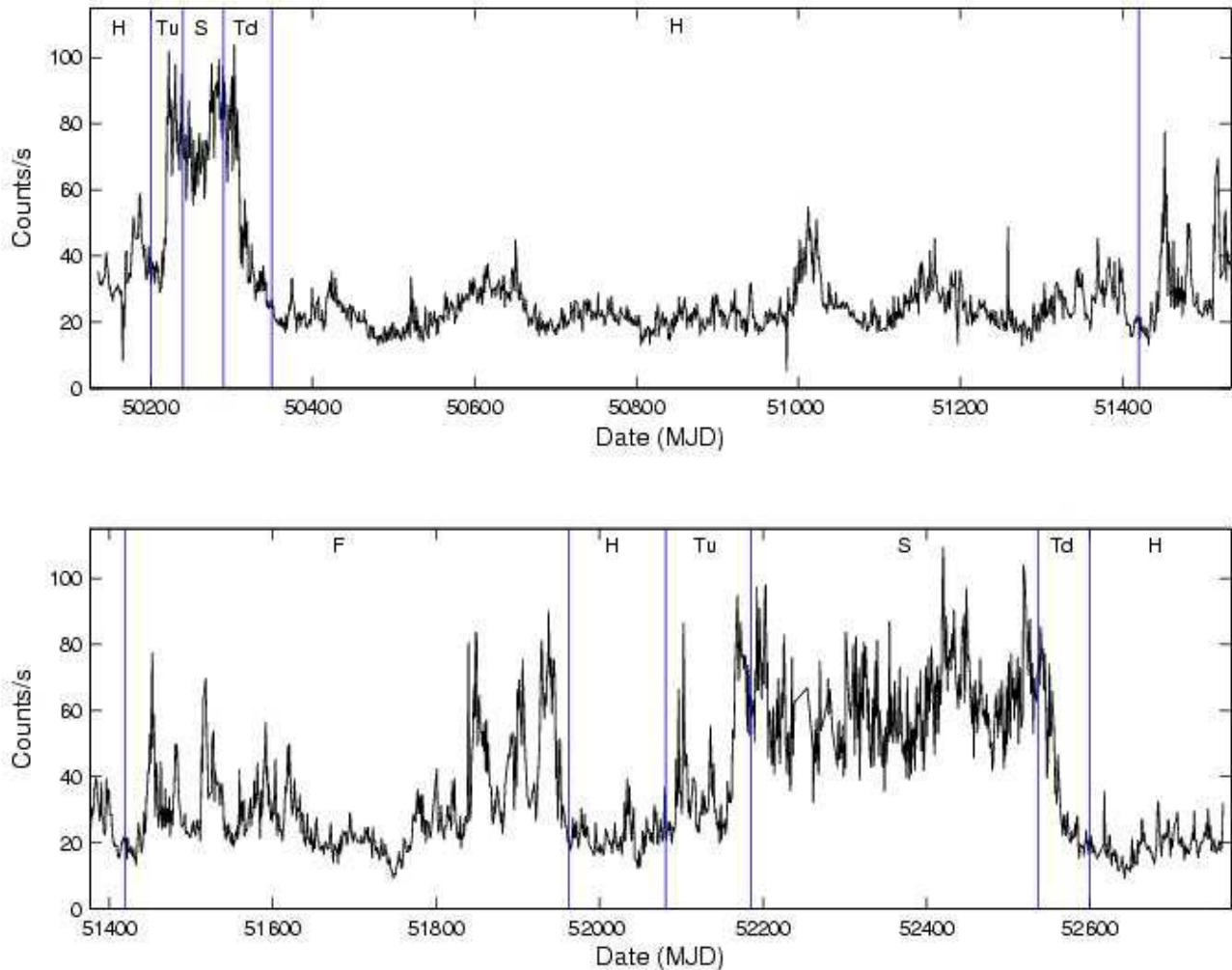


**Fig. 1.** ASM lightcurve for Cyg X-1 from MJD 50 135 (Feb 22, 1996) to MJD 52 763 (May 4, 2003). The different groups are marked in the plot, with *H* signifying hard state, *Tu* and *Td* transitions from hard to soft and soft to hard respectively, *S* the soft state and *F* signifies a period of large flares in the hard state.

to the difficulty are the large flares or ‘failed state transitions’, where the source appears to begin a transition but not complete it. We have chosen to call these episodes flares, and reserve the use of transition for cases when the source changes state. In this study we have attempted to use the PDS when determining the state of the source. For the canonical hard and soft states, there is no difficulty as their PDS are clearly separate and appear only in their respective state. The situation during the transitions (and flares) is by its very nature more ambiguous. In the following, we distinguish between hard and transitional state PDS by the power-law component appearing only in the latter. The same criterion is used to distinguish flares, with the difference between flares and transitions being that the source does not change state after a flare. The distinction between transitional and soft states is not as clear-cut. We have in this study assigned the PDS where the second Lorentzian component is not seen or significantly weaker than the first one to the soft state, along with the canonical PDS consisting only of the power-law component. In our classification, Fig. 2 is a hard state PDS, Fig. 3 a PDS from a flare or transition, and Figs. 4 to

6 soft state PDS. We shall compare this classification to others made from a spectral standpoint in Sect. 3.4.

#### 2.4. Hardness and Spectral Index

The energy spectrum of Cyg X-1 in the hard state can be represented as a soft thermal component and a hard power-law component with index  $\Gamma \sim 1.6$  and a high-energy cut-off. There is evidence of an iron fluorescence line at 6.4 keV and a broad Compton reflection component around 30 keV (e.g. Bałucińska-Church et al. 1995; Ebisawa et al. 1996; Gierliński et al. 1997). The soft state is dominated by a strong thermal component below  $\sim 3$  keV, combined with a power-law continuum extending above 1 MeV. The iron line is visible also in the soft state (e.g. Gierliński et al. 1999). The soft radiation is expected to come from an optically thick, geometrically thin accretion disc, while the hard emission is usually explained by a hot, optically thin medium where the soft disk photons are Comptonized (Shapiro et al. 1976; Poutanen 2001).

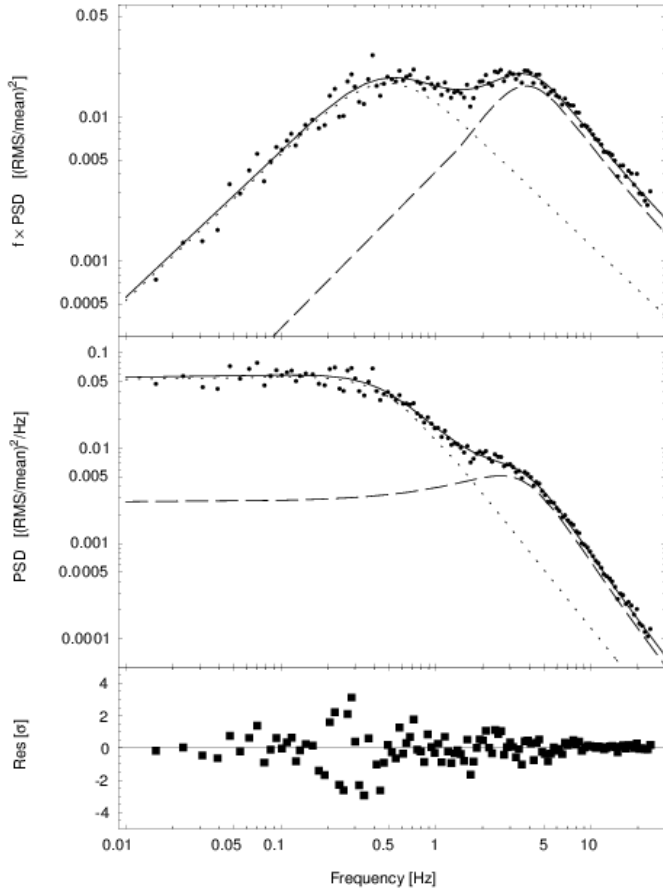


**Fig. 2.** Example of fit to hard state PDS using two Lorentzian profiles (model 1). This is the most frequent state of the PDS, and the majority of our observations are fit with this model. Hardness ratios ( $9 - 20 \text{ keV} / 2 - 4 \text{ keV}$ ) for this model fall in the range of  $0.50 - 1.1$ . The example is from an observation made on MJD 50 180.

We used the hardness ratios (or more specifically count ratios) between the 9–20 keV and 2–4 keV channels to provide a means of correlating the PDS properties with changes in the energy spectrum. To compute a hardness ratio, the 16 s lightcurves were first divided according to the start and stop times of the data used in each PDS. A mean count rate was then calculated in each energy range for each interval, and the hardness ratio  $HR$  computed. This way, each PDS could be tied to an average count rate and hardness ratio.

Figure 7 shows the flux-hardness relation. In Cyg X-1, the correlation between flux and hardness differs between the states. During the hard state it is generally negative, while in the soft state there is a positive correlation (Wen et al. 2001; Zdziarski et al. 2002). There is a distinct peak around  $HR \sim 0.3$ , indicating a rather sharp change in behavior.

The hardness as defined above is often a useful tool, as it provides an easy way to measure spectral changes with very good time resolution. However, it cannot readily be compared with hardness values from other instruments or energy bands. To facilitate comparison with other studies, we derived an empirical relation between our definition of hardness ratios and the spectral index  $\Gamma$ . This was done by modeling a number

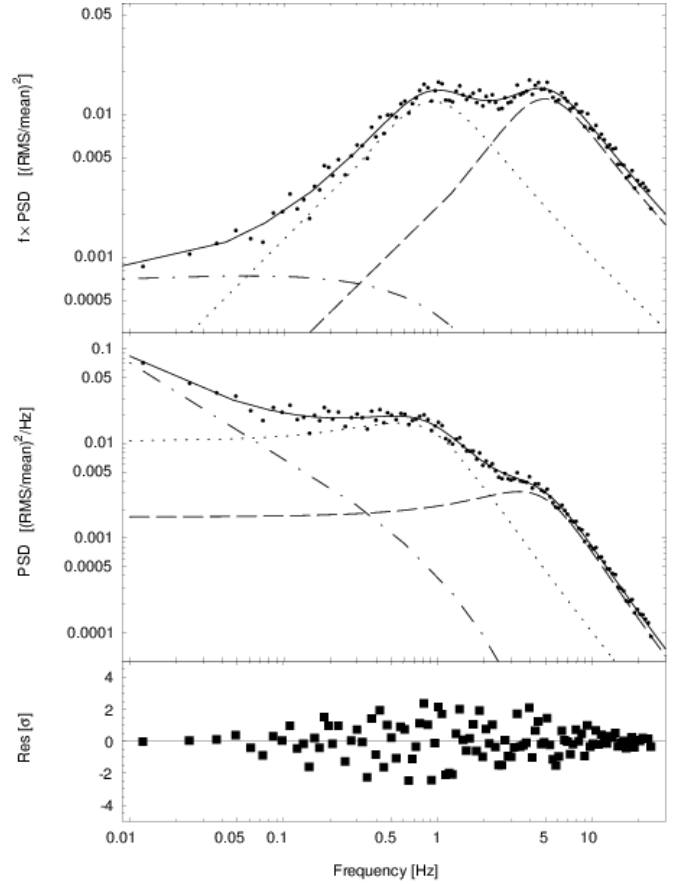


**Fig. 3.** Example of fit to a transition PDS using a cut-off power-law and two Lorentzian profiles (model 2). The PDS of Cyg X-1 take on this appearance during state transitions and larger flares in the hard state (failed transitions). Hardness ratios for these fittings fall in the range of  $0.25 - 0.45$ . The example is from an observation made on MJD 50 226.

of energy spectra in the 2–20 keV range with a power-law in `xspec`, as well as calculating their average hardness. While the energy spectrum of Cyg X-1, especially in the soft state, cannot accurately be described by a simple power-law, this approach provides a good approximation of the spectral characteristics of the source. The resulting empirical relation between the index  $\Gamma$  and hardness ratio  $HR$  was found to be well described by a power-law (see Fig. 8).

$$HR = 3.9 \times \Gamma^{-2.8} \quad (3)$$

The transitional state of Cyg X-1 has a typical index in the range  $2.1 \lesssim \Gamma \lesssim 2.4$  in the energy band 3–12 keV (Zdziarski et al. 2002; Fig. 3 in Zdziarski & Gierliński 2004). Comparing to the empirical relation of Eq. 3, this would correspond to a hardness  $0.3 \lesssim HR \lesssim 0.5$ , with the lower edge matching the peak in Fig. 7. The simplicity of the relation in Eq. 3 means that spectral index and hardness ratios can be used interchangeably, and we will consistently use the latter in this paper.

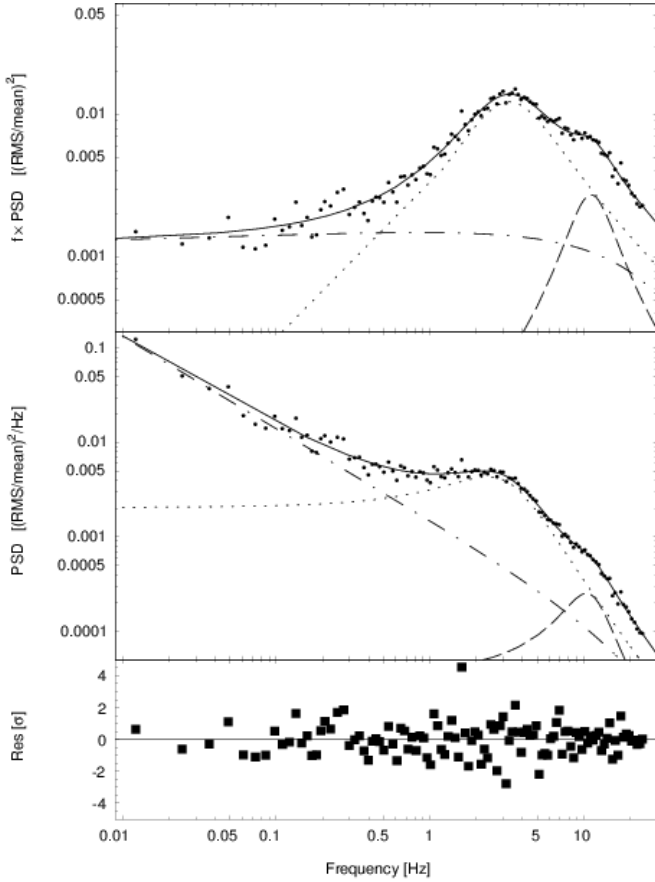


**Fig. 4.** Example of fit to soft state PDS using a cut-off power-law and two Lorentzian profiles (model 2). Almost 20 % of the soft state observations also allowed a fit with this model. The Lorentzian components have shifted compared to Fig. 3, and the power-law component extends to higher frequencies than during transitions. Hardness ratios for these fittings fall within the range of 0.20 – 0.30. The example is from an observation made on MJD 52 341.

### 3. Results

In this section we present the results of our analysis. We begin with a general description of how the PDS evolves during spectral transitions, and then describe in detail the relevant parameter correlations.

While narrow, well-defined peaks in the power spectrum are generally called QPOs, there is no set definition. This leads to a sliding scale where wider features are sometimes referred to as breaks and sometimes as QPOs. To avoid confusion and connection with the different types of physical processes associated with breaks and QPOs, we will consistently use ‘temporal feature’ or ‘characteristic frequency’ to describe the features seen in the PDS, and in the context of our modeling components refer to them as ‘Lorentzians’. For a review of temporal features in both BHC and NS systems, see van der Klis (1995, 2004). A possible identification of the different features in BHC in terms of those found in NS is presented by Klein-Wolt (2004).

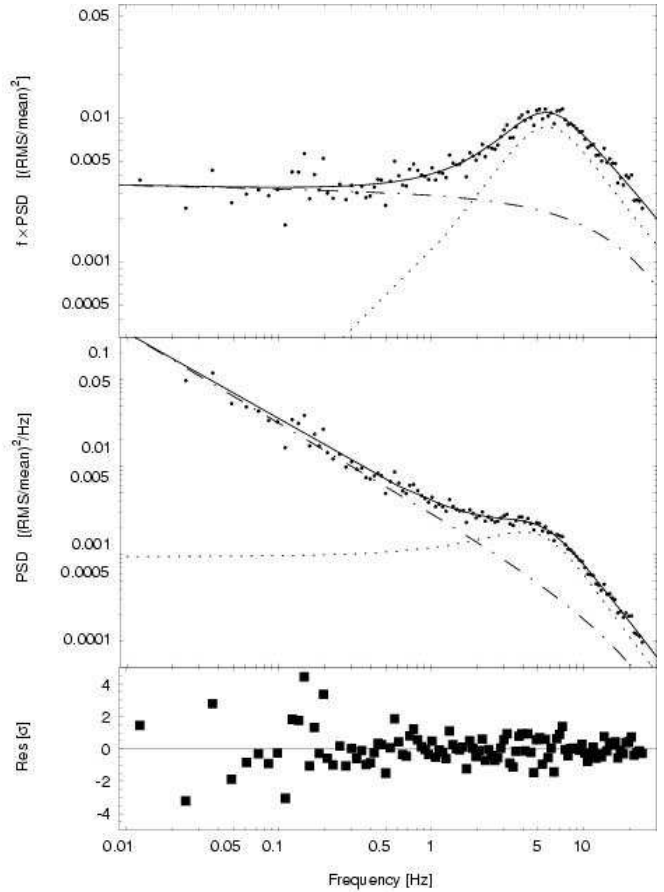


**Fig. 5.** Example of fit to soft state PDS using a cut-off power-law and one Lorentzian profile (model 3). Almost half the soft state observations allowed a fit using this model. Hardness values for this model fall in the range of 0.14 – 0.26. The example is from an observation made on MJD 52 341.

#### 3.1. PDS of the different states

As Cyg X-1 spends most time in the hard state, the majority of the observations were made during this state. It is well described by two Lorentzian profiles and no power-law component (see Fig. 2). The two peaks shift in frequency, moving on timescales of hours. In very few ( $\lesssim 1\%$ ) of the hard state cases, model 1 did not provide a good fit due to a third component being evident at higher frequencies. These cases correspond to the observations with highest hardness, and will be discussed further below.

During larger flares and transitions, the two peaks shift to higher frequencies and it becomes necessary to include the power-law component to achieve an acceptable fit. The power-law component only significantly contributes at lower frequencies (Fig. 3). When analyzing the data we separated flares, transitions from hard to soft state, and transitions from soft to hard state in an attempt to detect possible differences between them. However, in the analysis done in this paper the three appear identical. Our results on this point agree with those found previously (e.g. Pottschmidt et al. 2000; Cui et al. 2002; P03).

It is during the transitions and flares that the power spectrum of Cyg X-1 shows the most rapid changes. We are able

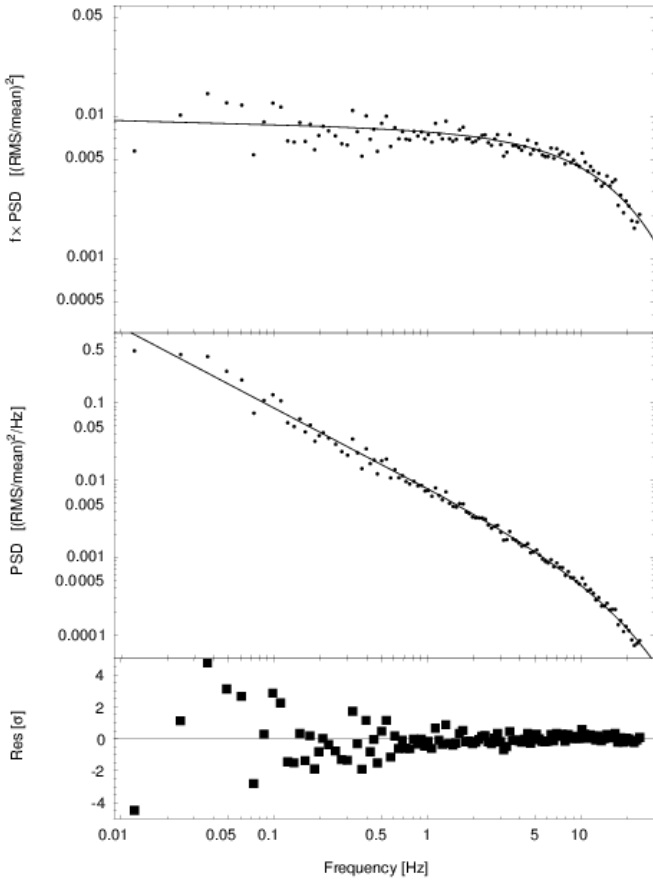


**Fig. 6.** Example of fit to soft state PDS using only a cut-off power-law (model 4). This is the canonical soft state PDS appearance for Cyg X-1, however only 35% of the observations made during the soft state allowed a fit using this model. Hardness values for this model fall in the range of 0.11 – 0.23. The example is from an observation made on MJD 52 257.

to see changes in the PDS down to our limit of  $\sim 15$  minutes, justifying our choice of a short integration time in the analysis.

In the soft state the power-law component dominates with an index close to  $-1$ . However, in the majority of the cases ( $\sim 65\%$ ), one or two Lorentzian components are needed in addition to the power-law in order to fit the PDS. The Lorentzian components are particularly frequent in the 2001/2002 extended soft state. During this period, the source made at least two brief transitions down to the hard state (also noted by P03). No trace of these transitions is seen in the ASM lightcurve of Fig. 1, but both the hardness and PDS reverted to that of the canonical hard state.

### 3.2. Relations between the peak frequencies

The relation between  $\nu_1$  and  $\nu_2$  is shown in Fig. 9. Our observations confirm the correlation between the peak frequencies of the PDS found in previous studies of Cyg X-1 in the hard state (N00; P03). Since our study is based on a much larger data set, we can make a more accurate analysis of the hard state frequency variations. We are also able to add the behavior of the peak frequencies during transitions, flares and into the soft

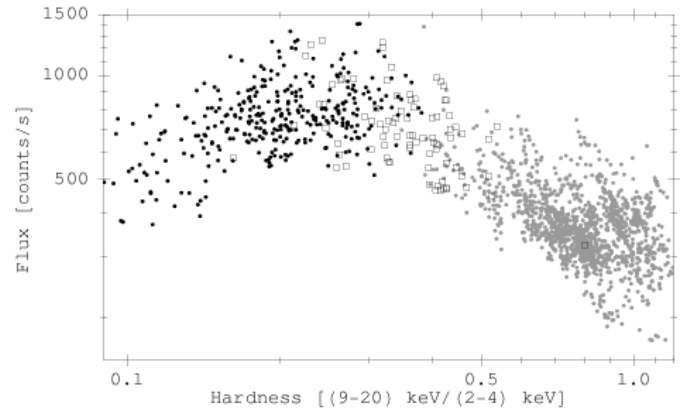


**Fig. 7.** Flux-hardness correlation of Cygnus X-1. Each point represents the mean values of hardness and flux during one PDS. Grey points are the hard state, black points the soft state and open squares points from transitions and flares. The change in correlation around  $HR \sim 0.3$  is clearly visible. The flux is the sum of the two channels.

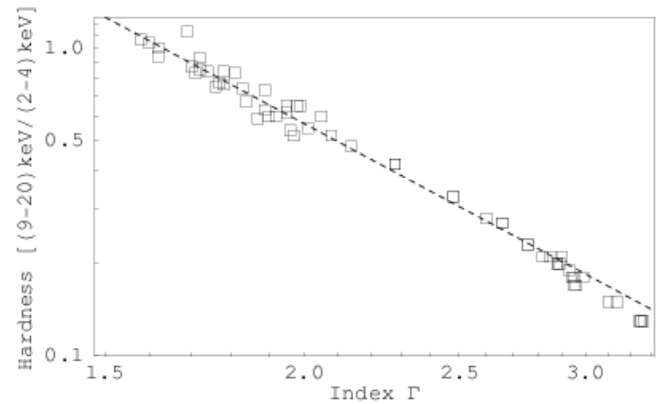


**Fig. 8.** Empirical relation between spectral index  $\Gamma$  and hardness  $HR$ , obtained by fitting the energy spectra between 2–20 keV with a power-law. Errors are within the boxes. The equation of the power-law is  $HR = 3.9 \times \Gamma^{-2.8}$ .

states. A clear feature in Fig. 9 is the steepening of the relation at  $\nu_2 \approx 5$  Hz. This corresponds to the region where the source goes from hard state into the intermediate/transitional state. We note that this is the region where P03 see a shift in power from their lower frequency Lorentzian ( $L_1$ ), to a higher frequency one ( $L_3$ ). Since we use only two Lorentzians, the break could in principle be attributed to a change in the components being fitted. We have however carefully monitored this region, and find no evidence of such a change in our data. Since our method of analysis allows us to detect changes in the PDS on timescales as short as  $\sim 15$  minutes, it is more likely that the break is due to a real change in the behavior of the components. The fact that the points lie in a continuous distribution, both in Fig. 9 and in the following figures, further supports this identification.

In the soft state, the relation between the two peak frequencies is somewhat uncertain. We see two major effects behind the large spread in these data. Since we do not correct the Poisson noise level for dead-time effects, our frequency range

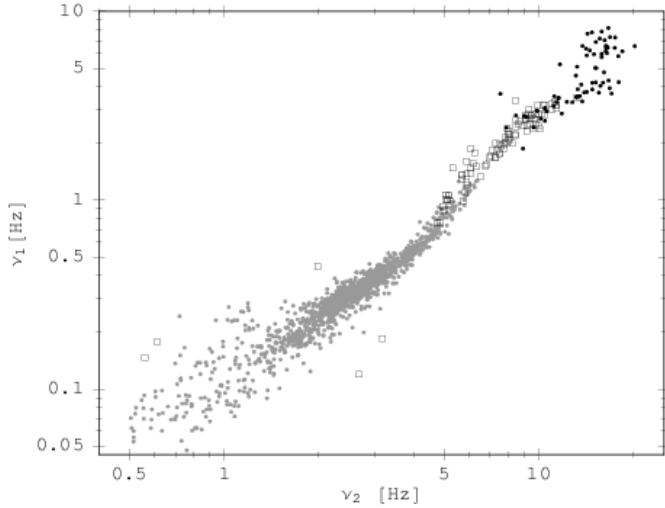


**Fig. 9.** Correlation between the peak frequencies of  $L_1$  and  $L_2$ . The gray and black points represent the hard and soft states respectively, and the open squares are the transition state. The break away from the hard state behavior as Cyg X-1 enters the transitional state is clearly visible.

is limited to the region where these can be neglected. As the second Lorentzian approaches our upper frequency limit of 25 Hz, it becomes difficult to constrain. Even with this rather conservative limit, we cannot rule out that the points near the limit are affected by dead-time effects. A second effect which further complicates the modeling is the fact that the power of the feature is reduced at higher frequencies. As we average over only ten power spectra, our signal-to-noise ratio does not allow us to model weak components. The spread of points in the soft state is therefore due to both the limitations set by dead-time effects and the signal-to-noise ratio.

### 3.3. Comparing the two Lorentzians

The strong correlation between the peak frequencies of the two Lorentzians in Fig. 9 suggests a close physical link between the components. However, when studying the relations between  $W_i$  and  $\nu_i$  the two components show completely different behavior (Figs. 10 and 11 respectively). The first Lorentzian shows no correlation between these parameters, and  $W_1$  remains fairly constant. For the second Lorentzian,  $W_2$  changes roughly two orders of magnitude, and there is a strong correlation, which can approximately be described by a power-law with index  $\sim -1.5$ . In contrast with the relation in Fig. 9, the points for the transitional and soft states seem to follow the same relation as in the hard state.

During the hard state there are cases where the Lorentzians shift to very low frequencies. These cases correspond to observations with very low flux and a high hardness ratio. To provide a good fit in these cases, we found it necessary to freeze the ratio between the peak frequencies by extrapolating the relation found at higher frequencies (see Sect. 4.2 below). For these low frequencies in the hard state, there is a hint of flattening of the index in the  $W_2$ - $\nu_2$  correlation (open triangles). Since this oc-

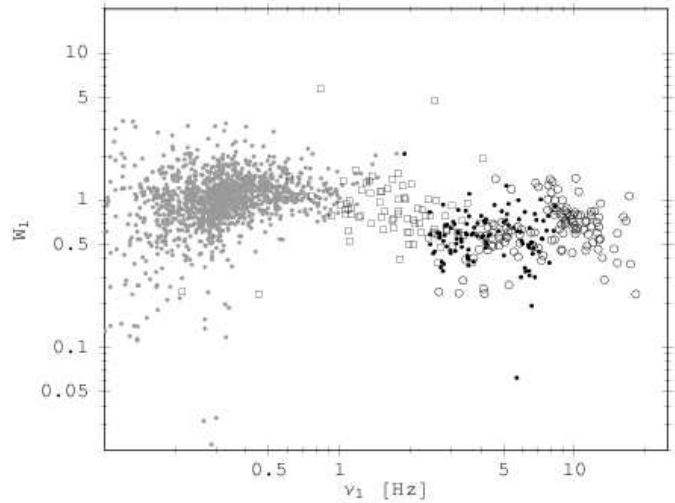


**Fig. 10.** Relation between  $W_1$  and  $\nu_1$ . Symbols are the same as in Fig. 9, with open circles being points from the single Lorentzian in model 3. The width is generally constant throughout the frequency range.

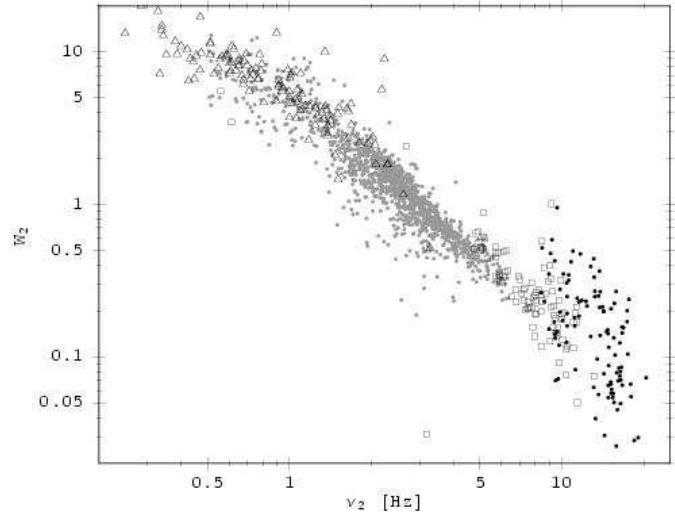


**Fig. 11.** Relation between  $W_2$  and  $\nu_2$ . Symbols are the same as in Fig. 9, with open triangles being points from the hard state where the relation between  $\nu_1$  and  $\nu_2$  was fixed. The negative correlation between  $W_2$  and  $\nu_2$  is clear, and can approximately be described by a power-law with index  $\sim -1.5$ .

curs in the region where  $\nu_1$  was fixed in relation to  $\nu_2$  we cannot rule out that this is an artifact of the fitting procedure.

In Fig. 10, the open circles represent the single Lorentzian of model 3 (see Table 2). We identify this component as  $L_1$ . The identification is supported by the fact that the points from this component well matches the other soft state points, both in this and subsequent figures. If the component is instead identified as  $L_2$ , the distributions occupy completely separate regions in the parameter space. We surmise that as both Lorentzians move up in frequency, eventually  $L_2$  becomes too weak and moves too high in frequency for us to see in our analysis, and only  $L_1$  is visible.



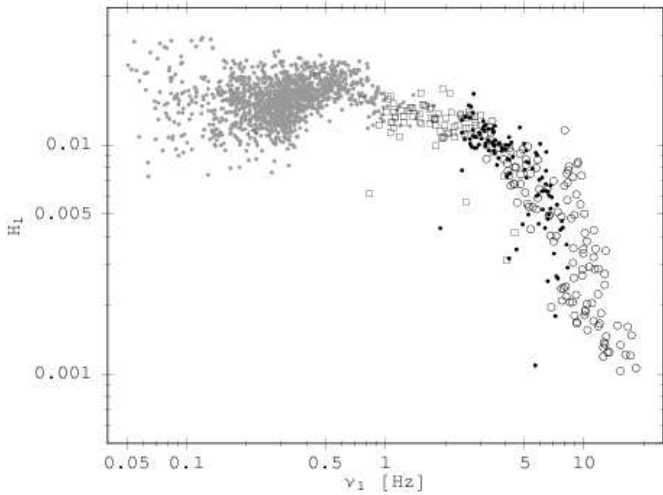


**Fig. 12.** Power at the peak frequency versus peak frequency for  $L_1$ . Symbols are the same as in Fig. 10. The change in behavior during and after the transition (open squares) is rather gradual.

Comparing the relations between  $H_i$  and  $\nu_i$  shows similar behavior for  $L_1$  and  $L_2$  (Figs. 12 and 13). Both components stay at roughly constant height at lower frequencies, and decrease rapidly with frequency at higher  $\nu_i$ . This change in behavior for  $L_2$  occurs as Cyg X-1 enters the transitional state, suggesting that the mechanism behind  $L_2$  starts to weaken as the transition begins, perhaps due to a change in the accretion geometry. We surmise that the behavior of  $H_1$  at lower frequencies is most likely explained by the effect first noted by Belloni & Hasinger (1990) in their analysis of the PDS in terms of a doubly broken power-law model. They found a negative correlation between the frequency of the first break and the power at that frequency. Transforming this correlation into the  $fP_f$  representation leads to approximately constant  $H_1$  as a function of  $\nu_1$ . Our results are also consistent with the relation between normalization and peak frequencies of the Lorentzian components seen in Fig. 6 of P03, but note the difference in parameters used and identification of components.

Combining the behavior of  $H_i$  and  $W_i$  once again shows the difference between the two components. Since both  $H_1$  and  $W_1$  stay roughly constant at low  $\nu_1$ , the contribution from  $L_1$  to the total RMS variability remains the same, weakening only above  $\sim 5$  Hz, when the source is in the soft state. In contrast, the RMS contribution from  $L_2$  falls with  $\nu_2$  over the whole frequency range. As  $H_2$  starts to decrease,  $L_2$  weakens very rapidly. Interesting is also that the rapid decrease in height starts at  $H_i \sim 5$  Hz for both  $L_1$  and  $L_2$ . A possible explanation for the similarities and differences in behavior of the components will be presented in Sect. 4.3.

### 3.4. Evolution of the PDS

As described above in Sect. 3.1, there are systematic changes in the PDS tied to the changes in hardness. Figures 14 and 15 show the evolution of  $\nu_i$  with hardness. Both peak frequencies increase with decreasing hardness. This movement follows ap-

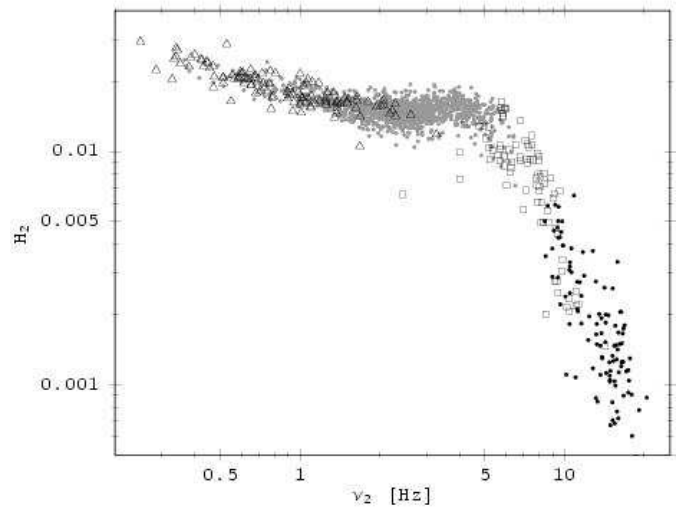


**Fig. 13.** Power at the peak frequency versus peak frequency for  $L_2$ . Symbols are the same as in Fig. 11. Note the sudden change in behavior as the source enters the transitions (open squares). This suggests the underlying physical mechanism reacts sharply to changes, e.g. in the accretion geometry, occurring at these periods.

proximately the same pattern in all states while the components are detectable, which we take as another indication that we are following the same two components in all cases. We note that this gradual increase in peak frequency would be expected if the Lorentzian components are assumed to arise in a region that is closer to the central object in the soft state than in the hard state (e.g. the inner edge of a truncated accretion disk or a transition region between disk and corona). Such models have been presented by e.g. Poutanen et al. (1997), Churazov et al. (2001), and Zdziarski et al. (2002).

Beyond the necessity to include the power-law component in our models below a hardness of  $\sim 0.4$ , Figs. 14 and 15 show no change in behavior around the transition phase hardness,  $HR \sim 0.3$  seen in Fig. 7. We therefore conclude that the changes responsible for altering the flux-hardness correlation do not affect the movement of the peak frequencies. The other parameters do not show any evolution with hardness, beyond a trend for the power-law to extend to higher frequencies as the hardness decreases. This is a natural effect of the model as the Lorentzian components move away from the lower frequencies. The behavior is however consistent with the  $f^{-1}$  power-law gradually extending higher in frequency as the source goes from hard state to soft state (Zdziarski et al. 2004).

When determining the state of the source, we have done so from the point of view of the PDS, as they are the base of our analysis. Figures 14 and 15 show that there is a unique relation between a point in the PDS parameter space and the hardness. We are therefore able to compare the ‘PDS states’ with definitions based on the spectral index of the source. We see that our transitional state PDS roughly fall in the range  $0.3 \lesssim HR \lesssim 0.5$ . Below this range is the soft state and above the hard state. From the relation in Eq. 3, the corresponding range in spectral index is  $2.1 \lesssim \Gamma \lesssim 2.4$ , with the hard state having a lower and the

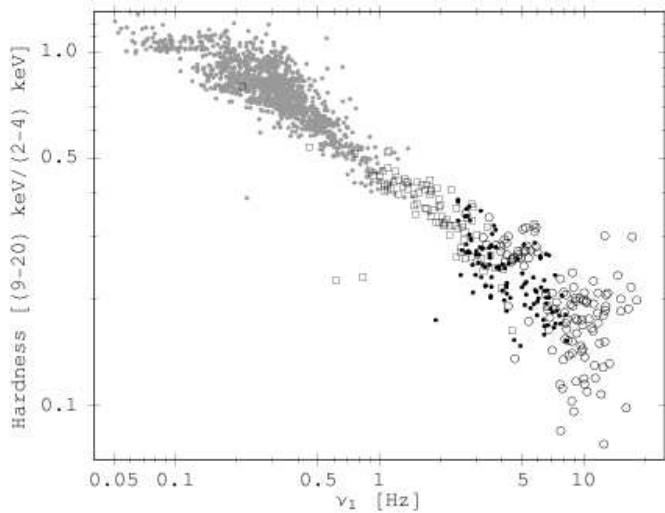


**Fig. 14.** Relation between hardness and  $\nu_1$ . The symbols are the same as in Fig. 10. There is no apparent change in behavior as the source enters the transitional or soft states.

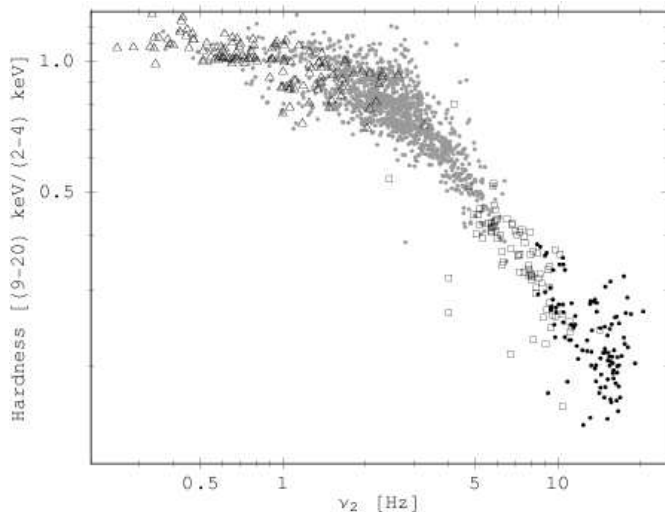


**Fig. 15.** Relation between hardness and  $\nu_2$ . The symbols are the same as in Fig. 11. Note the tendency for the hardness to ‘flatten out’ at  $\sim 1.1$ .

soft state a higher index. We note however, that these boundaries are not strict, and that there is some overlap between the different states. This range matches well with previous results, e.g. Zdziarski et al. (2002); Zdziarski & Gierliński (2004).

To illustrate the complete evolution of the PDS, Fig. 16 presents a series of fittings showing the gradual change from normal hard state to canonical soft state PDS. Unfortunately, the observations made did not capture the complete evolution in a chronological series, so Fig. 16 is a montage of PDS from observations made during a brief transition to the hard state in the extended soft state of 2001/2002. The top three panels are from observations made on MJD 52 330 and panels **d** and **e** are from an observation made on MJD 52 324. The last PDS (panel **f**) is made on MJD 52 358, when the source had once again returned to the soft state. Figure 16 illustrates the shift in the peak

frequencies of the Lorentzians, and the gradual increase of the power-law as the source goes from hard state to soft state.

## 4. Discussion

The results of our analysis show that the PDS of Cyg X-1 can be successfully modeled in all the spectral states using only a few components. The observed behavior of the Lorentzian components lends weight to the argument that they indeed represent the temporal characteristics of the physical processes giving rise to the PDS.

### 4.1. Identification of components

As noted in Sect. 3.2, the identification of components in the PDS is not trivial. P03 in their study use four Lorentzians to fit the power spectrum. While their fourth component,  $L_4$ , is above our upper frequency limit, our model will fit the two dominating components at a given time. According to the identification of P03 this means that in the canonical hard state we fit their first two Lorentzians, but in the larger flares and transitions we fit their second and third Lorentzians. The first Lorentzian is then quite weak and will be ‘absorbed’ in our power-law component. Supporting this identification is the change in the correlation of the peak frequencies during transitions and large flares.

Recently, van Straaten (2004) has argued that the identification of P03 leads to significant deviations during ‘failed state transitions’. For canonical hard state PDS, the first two Lorentzians dominate and follow the relation of Fig. 17, but van Straaten (2004) points out that if the second and third components dominate in transitions and large flares, the peak frequencies of the first two components deviate significantly from the correlation in the normal hard state. If instead the dominating components are still identified as the first two Lorentzians, the peak frequencies will follow the trend seen in Fig. 17. Although the points do not lie along the extension of the power-law described at lower frequencies, their behavior matches that of the other sources, as seen in Wijnands & van der Klis (1999). To support the identification, van Straaten (2004) adds data from a flaring episode in November 2000, but a gap between the canonical hard state PDS and these flares still remains.

Since the study reported here allows for shorter timescales to be monitored, we are able to follow changes in the Lorentzians in great detail. From Fig. 16 it is clear that our model can explain the evolution of the PDS, and provide extensive coverage of all states of the source. As seen in Fig. 11 our results show a continuous distribution between the hard state and transitions, and we are able to fill in the gap in the data of van Straaten (2004). The results here therefore favor this identification over that of P03.

### 4.2. Comparisons with models

The temporal features observed here have been detected both in NS and BHC systems. The origin of these characteristic

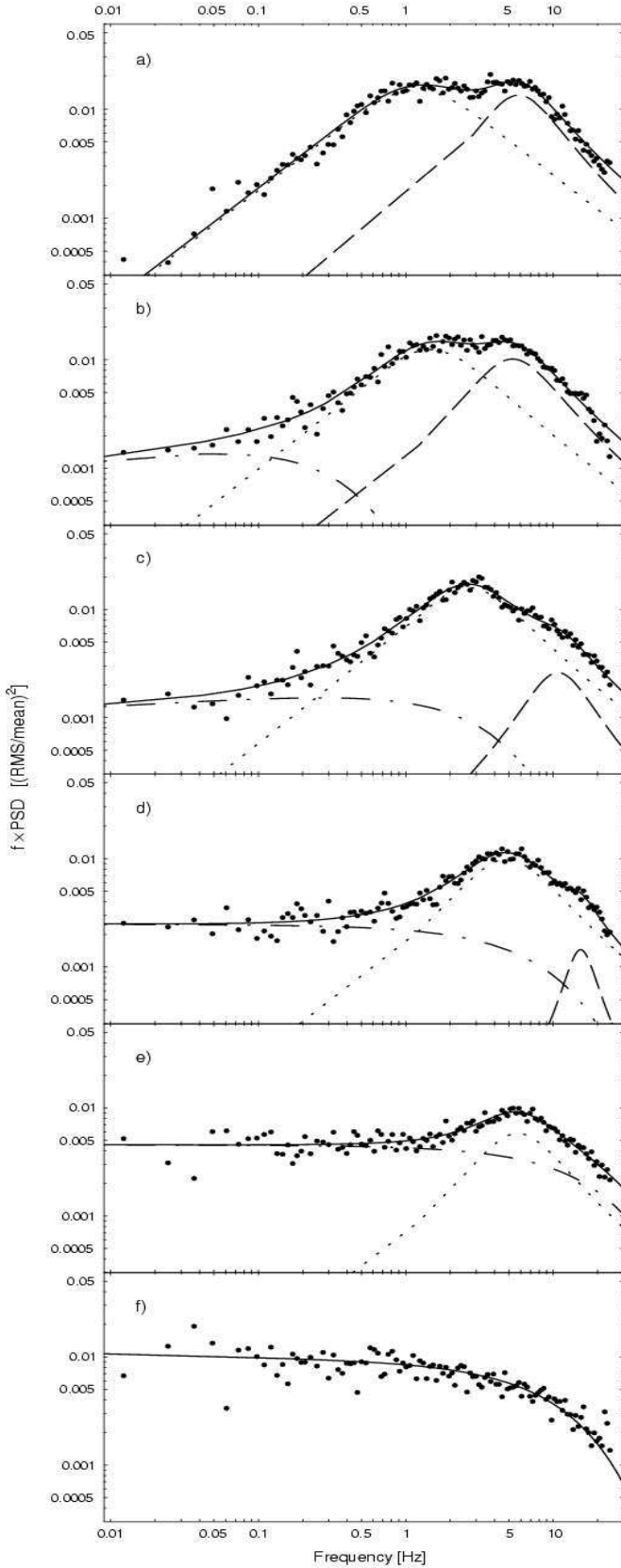


**Fig. 16.** Montage showing the evolution of the PDS of Cyg X-1 from hard state (panel **a**) to canonical soft state (panel **f**). The top three panels (**a-c**) are from observations made within a few hours during MJD 52 330, and clearly illustrate the changes that can occur on this timescale. Panels **d** and **e** are from MJD 52 324, and are also no more than a few hours apart. The bottom panel (**f**) is from an observation on MJD 52 358. Note the weakening and narrowing of the upper frequency Lorentzian (dashed line) as it shifts to higher frequencies.

frequencies has been long debated in the literature, and various models have been proposed in each physical scenario (for an extensive review, see van der Klis 2004). However, recent comparative studies between these two types of sources have shown that they present very similar frequency correlations, over a frequency range of many decades (Psaltis et al. 1999; Belloni et al. 2002). The similarities suggest the same underlying physical mechanism, which cannot be dependent on either a magnetosphere, a solid surface, or an event horizon (Wijnands 2001). Beat-frequency models, which have been extensively used in the context of NS, can not easily be extended to black holes as these are unable to provide an anchor to the magnetic field, a condition that is needed to generate a beating with the Keplerian frequency.

Several classes of models have been proposed to explain the observed QPO's and their correlations (see Psaltis et al. 1999, and references therein). They commonly ascribe the variations to processes in the accretion disk. This can be done by identifying observed frequencies with orbital, epicyclic and precessional frequencies at certain radii (such as the inner edge of the disk). Another approach is to study disk oscillation modes. For example, in the region close to the compact object, global disk oscillation modes can become trapped in particular disk annuli. For comprehensive summaries on this topic, see e.g. Wagoner (1999) and Kato (2001). As demonstrated in Wagoner et al. (2001), disk mode frequencies are mainly determined by the mass and angular momentum of the compact object, and depend only weakly on the disk parameters. While this property makes the models good candidates in explaining the high coherence seen in higher frequency QPO's (Barret et al. 2004), it also makes it difficult to explain the large (over one order of magnitude) shifts in peak frequency observed in our study. In addition, the features we model with Lorentzians have low coherence. Our parametrization does not directly give a value for the more generally quoted quality factor  $Q = \nu/\Delta\nu$ , but for  $L_1$  this value is  $\lesssim 1$  in all states. For  $L_2$ ,  $Q$  varies with the spectral state. It is low ( $Q < 1$ ) in the hard state and while higher in the soft state,  $Q < 5$  in all observations.

In the following, we will consider the somewhat idealized case of the relativistic precession model (RPM, Stella & Vietri 1998, 1999). It states that the timing features are the observable effect of the relativistic nodal and periastron precessions of a disk element or a 'blob' in a slightly tilted and eccentric orbit, respectively. Equally possible is the interpretation of the features arising in a narrow band or annulus in the inner region of the accretion disk (see e.g. van der Klis 2004). Although the predicted frequencies are those for free particle orbits, these can still often be recognized in the models of disk modes (e.g. Wagoner 1999). Psaltis & Norman (2000) showed that a sharp transition region in the accretion disk acts as a low-band pass filter with strong resonances near the frequencies predicted by the RPM, motivating a closer look at this model. Stella, Vietri, & Morsink (1999, hereafter SVM) have shown good agreement between the predicted frequency correlations in the RPM model and a small number of BHC and NS observations. Although the model currently requires NS spin rates and masses higher than measured, these problems are dependent on the chosen equation of state, and the RPM

model successfully predicts the observed quadratic dependencies between lower and higher frequency features seen in many sources (see van der Klis 2004, and references therein). Based on previous calculations (by Bardeen et al. 1972; Okazaki et al. 1987; Kato 1990) of the Keplerian  $\nu_\phi$ , epicyclic  $\nu_r$ , and vertical  $\nu_\theta$  frequencies for a Kerr black hole, SVM derived that in the weak field approximation for a slowly rotating black hole

$$\nu_{\text{nod}} \propto a_* M^{1/5} \nu_{\text{per}}^{6/5}, \quad (4)$$

where  $\nu_{\text{nod}} = \nu_\phi - \nu_\theta$  is the nodal precession frequency,  $\nu_{\text{per}} = \nu_\phi - \nu_r$  is the periastron precession frequency,  $M$  is the mass, and  $a_* = a/R_g$  is the dimensionless specific angular momentum (with  $a = J/Mc$ ,  $R_g = GM/c^2$  being the gravitational radius,  $J$  the angular momentum,  $c$  the speed of light in vacuum, and  $G$  the universal gravitational constant). We used a power-law model to fit the correlation between frequencies for the hard state data (see Fig. 17), up to the *break* observed in the transitional state at  $\nu_2 \simeq 5$  Hz. The best-fit parameters did not change significantly selecting a somewhat smaller, more conservative upper limit, nor was the fit affected by ignoring the points at the lowest frequencies. We obtained a power-law index  $1.20 \pm 0.01$  in remarkably close agreement with Eq. 4.

In SVM it is argued that due to the geometry of a tilted inner disk, the second harmonic of the nodal precession frequency gives the strongest modulation, and that this assumption provides the best match for their observations. We also found that a good fit of our data using the  $\nu_1 = \nu_{\text{nod}}$  identification would only be possible for an unrealistically large black hole mass. Adopting the SVM identification, i.e. in our case  $\nu_1 = 2\nu_{\text{nod}}$  and  $\nu_2 = \nu_{\text{per}}$ , and using the full relativistic expressions for the precessional frequencies, it is possible to derive some of the physical parameters of the system. For this purpose we used the  $M = 8M_\odot$  mass estimate (see Nowak et al. 1999, and references therein). Although this  $M$  value is somewhat uncertain, the frequency relation depends weakly on the black hole mass as shown by Eq. 4. At this frequency range, there are two possible solutions for the specific angular momentum  $a_*$ , depending on whether the orbital motion is prograde or retrograde. We obtained  $a_* = +0.49 \pm 0.01$  and  $a_* = -0.57 \pm 0.01$  respectively, comparable to previous results based on modeling of energy spectra (see e.g. Shapiro & Lightman 1976; Zhang et al. 1997). In Fig. 17 the best fit for the prograde case is shown (*solid line*), and some derived orbital radii are indicated. During the hard state, within the assumptions of the RPM, the inner radius  $R_{\text{in}}$  of the disk ranges from 50 to 22  $R_g$  when reaching the transitional zone. If the retrograde case is instead assumed the corresponding values change very little, with the inner disk ranging from 55 to 25  $R_g$ . These ranges are in very good agreement with coronal model estimates for Cyg X-1 (see di Matteo & Psaltis 1999, and references therein).

The behavior during the transitional and soft states seems to be more complex, in part because of the spread of the data points at the highest frequencies. If all the data above the break is modeled with a second power-law (thus given an index  $1.7 \pm 0.03$ ) the fit residuals clearly do not appear randomly distributed. Another possible interpretation of the data is that after the transition, the points corresponding to the soft state follow a power-law with an index identical to that of the hard state. This

picture is reinforced when comparing our Cyg X-1 RXTE data to those presented in a study of the frequency correlations in X-ray binaries by Wijnands & van der Klis (1999), from many different NS and BHC sources (open squares in Fig. 17). The data points seem to lie along ‘parallel tracks’ as predicted by the RPM. This behavior, along with the gradual shift between the two tracks during the transitional state, must then be explained. It seems likely that a reconfiguration of the accretion disk geometry during the state transitions is responsible for the changes in the relation between the frequencies.

A suggestion to explain the state transitions in Cyg X-1, first made by Shapiro & Lightman (1976) and later on by Zhang et al. (1997), is that they are produced by the reversal of the disk rotation. This would occur due to the unstable nature of the stellar wind from the primary star feeding the accretion. In this scenario, the system would switch back and forth from a retrograde rotation in the hard/low state, to a prograde rotation in the soft/high state. Differences in luminosity would be explained by the changes in the ‘last stable orbit’  $R_{\text{last}}$ , that in the case of maximal rotation would change from  $R_{\text{last}}(a_* = -1) = 9R_g$  to  $R_{\text{last}}(a_* = +1) = R_g$ . According to our previous fit of the hard state data, a reversal of the disk rotation would imply that  $a_* = +0.57$  in the soft state. However, this value does not fit the soft state data. SVM showed that corrections for non-negligible eccentricities or tilt angles are generally small. Very large eccentricities ( $e > 0.85$ ) would need to be invoked to explain the data. The rotation reversal scenario could thus only be maintained with additional assumptions.

Reducing the spread of points in the soft state data could help determine the behavior of the relation and thereby further constrain models. A more thorough study of the soft state data, extending to higher frequencies, is currently underway. This analysis will also make use of data recently made public from an additional soft state in June/July 2003.

### 4.3. Behavior of components

As noted by Belloni et al. (2002), when using Lorentzian components to model both broad and narrow features in the power spectrum, the peak frequency  $\nu_i$  does not have an immediate interpretation in the picture of a damped harmonic oscillator. Interpreting the features as arising by superpositions of a range of frequencies (such as from an annulus in the innermost region of the accretion disk),  $\nu_i$  instead becomes a measure for the highest frequency contributing, or the one contributing the most power. Our width parameter  $W_i$  can then be seen more as a measure of the extent of the contributing region, than as a measure of the lifetime of an individual process. For a deeper discussion on this topic, see Belloni et al. (2002).

The different behaviors of the width parameter  $W_i$  in the two components directly rule out the simple case of the components originating in the same ‘blob’. If the Lorentzians instead arise in an annulus close to the inner radius  $R_{\text{in}}$  of the accretion disk, increasing  $\nu_i$  indicate decreasing  $R_{\text{in}}$ . The decrease of  $W_2$  with frequency may then be understood by a more narrow annulus dominating the radiation at smaller  $R_{\text{in}}$ . However,  $W_1$  is roughly constant as  $\nu_1$  increases. If the two components arise

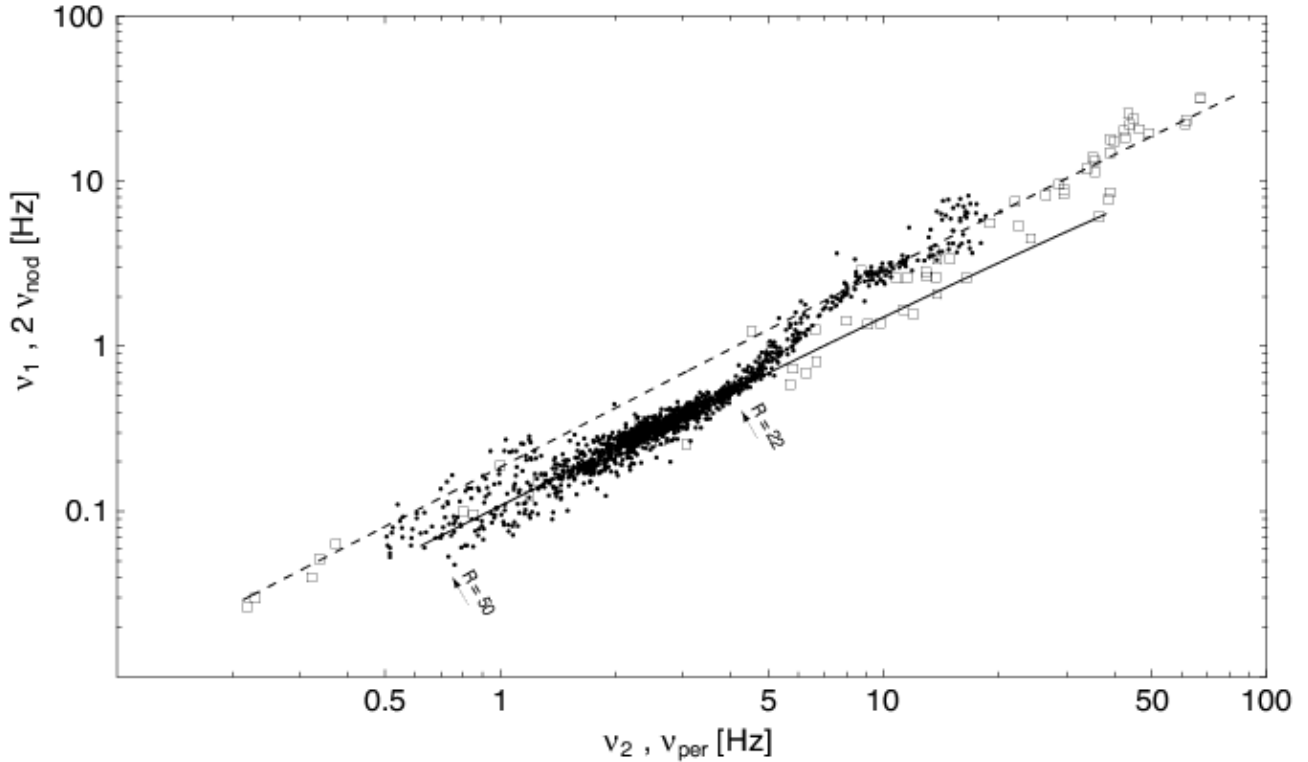


**Fig. 17.** Relation between peak frequencies (black points) together with the fit to the relation predicted in the relativistic precession model of Stella & Vietri (1998, 1999). Also plotted are the points from Fig. 2a in Wijnands & van der Klis (1999) (open boxes), with data from both neutron star (atoll sources) and BHC sources. The arrows mark different inner radii of the accretion disk, in units of gravitational radii. The solid line is the fit to the 1230 hard state points in the case of prograde rotation, when  $\nu_1 = 2\nu_{\text{nod}}$ . The best-fit power-law has an index of  $1.20 \pm 0.01$ . As the source enters the transitional state, the relation clearly breaks away from that predicted by the RPM model. The dashed line corresponds to a power-law of index 1.20 shifted to approximately follow the points from the soft state.

in the same annulus,  $W_1$  may be expected to behave in the same way as  $W_2$ . As can be seen in Figs. 10 and 11, this is not the case. Any model in which the two components arise from the same annulus then requires a mechanism allowing  $L_1$  to show different behavior than  $L_2$ . In the context of the RPM, where  $L_1$  is identified as the nodal frequency, a possible explanation is that warping of the disk leads to a smaller deviation from the orbital plane at smaller  $R_{\text{in}}$ . This would lead to the modulation decreasing with decreasing  $R_{\text{in}}$ , thus compensating for the dominance of the innermost ring in terms of emitted radiation. The result would be a larger ‘effective’ annulus contributing to  $L_1$  than to  $L_2$ , which is dominated by the narrow innermost region. For  $L_1$ , the net effect must be an approximately constant width as seen in Fig. 11. We note that during the hard state,  $R_{\text{in}}$  decreases by about a factor of 2 (Fig. 17), while the flux increases with approximately the same factor (Fig. 7), suggesting a  $\sim 1/R_{\text{in}}$  relation. If the deformation of the disk scales as  $R$ , the net effect would be consistent with a constant power of the component as seen for  $L_1$ . If this simple picture is true,  $L_1$  could provide important constraints on the geometry of the accretion disk close to  $R_{\text{in}}$ .

The argument used for the different behaviors of  $W_1$  and  $W_2$  can also be extended to the case of  $H_i$  during transitions (Figs. 12 and 13).  $H_2$  starts decreasing rapidly as the transition

period starts, whereas  $H_1$  shows a more gradual reaction. If the transitional stage is considered to be a phase of rapid changes in the accretion geometry, a feature arising from a narrow ‘ring’ will react more sharply than one originating in a wider disk annulus. After the transition both Lorentzians show the same behavior, indicating that the geometry once again becomes more stable. Since the normalization used gives the relative power of different components, it is natural that as the Lorentzians shift to higher frequencies, the power-law component will start to dominate the PDS. The decrease in power of the Lorentzians will then mainly be a decrease in relative strength, rather than an intrinsic weakening of the physical processes giving rise to the components. We note that this scenario is also a possible explanation for the changes in the frequency correlation in Fig. 17 during transitions. During the transition the changes in accretion geometry disturb the relation between the peak frequencies, but as the source settles into the soft state the correlation is resumed. An explanation must still be found for the difference between hard and soft state, e.g. large deviations from a circular orbit or a shift from the second to higher harmonics.

The decrease of  $W_2$  with peak frequency is also interesting when comparing narrow QPOs with broader features (such as breaks or ‘humps’). Psaltis et al. (1999) observe that whereas so-called lower kHz QPOs seen in neutron star sources are

narrow well-defined peaks, components identified as the lower kHz QPO at much lower frequencies are broader. As our observations of  $L_2$  indicate, studies such as this one have the potential to show the complete evolution from the broader features at low frequencies to narrow QPOs at high frequencies. Tracking these components will determine whether they indeed originate from the same process.

A feature seen especially in Fig. 15 is the tendency for the hardness to ‘flatten out’ at a value  $HR \sim 1.1$ . Cyg X-1 only reaches these levels of hardness in observations with very low flux. The behavior of the hardness at these times could be explained by the index of the power-law component in the energy spectrum ( $\Gamma$ ) reaching a minimum value, and changes in flux (and thereby the PDS) arising from another component, e.g. small flares. If the variations of  $\Gamma$  are attributed to variations in the accretion disk rather than the hot inner flow/corona (e.g. Zdziarski et al. 2002), the ‘flattening’ of the hardness could be seen when these variation reached some outer boundary, and changes in flux were instead due to smaller variations in the processing of the soft input photons. That the peak frequencies of the Lorentzian components also vary at these times might suggest they are related to the corona rather than the accretion disk. Arguments for relating ‘breaks’ or QPO features in Cyg X-1 to a transition region at the inner edge of the disk or to the corona have been presented by e.g. Churazov et al. (2001) and P03. However, we note that this behavior can also be explained by variations in the local disk accretion rate. Such a mechanism has been suggested by Zdziarski et al. (2002) to explain variations in amplitude of the hard state energy spectrum with no change in shape, i.e. roughly constant  $\Gamma$ .

As stated in Sect. 2.3, during the observations with lowest flux we froze the relation between  $\nu_1$  and  $\nu_2$  according to the solid line in Fig. 17. The flux of these observations were typically below  $\sim 500$  counts/s in the 2-9 keV range, and the hardness was  $HR \gtrsim 1$ . The vast majority of these observations were made between MJD 50 400 and MJD 51 000 (November 1996 – July 1998, cf. Fig. 1), and constitute  $\leq 10\%$  of the hard state observations. During these low flux observations, we could also see an excess above 10 Hz in almost half the cases. This may well be a third component, which we only see the times it has moved to the lower edge of its frequency range. In observations with a more typical flux level it moves too high in frequency to be detected in our analysis. We surmise this is the highest frequency component seen by N00, and  $L_4$  in P03. This feature could add to the spread of points at low  $\nu_i$ , but does not otherwise affect our results.

## 5. Conclusions

After more than eight years of observations, the RXTE data archive is an excellent source for long-term studies. Using data from this archive we were able to follow the evolution of the PDS of Cyg X-1 from February 1996 to May 2003. By choosing a simple yet flexible approach for our analysis we could model the major features in all states with only three components. Our method also allowed us to detect changes in the power spectrum on timescales as short as  $\sim 15$  minutes.

Our analysis provides several new results. The main result is the successful modeling of the PDS of Cyg X-1 through all the states. We prove that our choice of models and parameters successfully enables us to show a natural transition from hard state to intermediate to soft state and back, and also allows us to study the behavior of the Lorentzian components in detail. The combination highlights new correlations between the parameters with interesting physical interpretations.

We find that the spectral state of the source can be uniquely determined from the parameters of the Lorentzian components. The parameters used here are the width  $W_i$  and peak frequency  $\nu_i$  of the Lorentzians, along with the power at the peak frequency,  $H_i$ . The correlations between parameters can all be described by continuous functions, which differ between components. This is most evident when comparing Figs. 11 and 10. While the correlations between the peak frequencies and between  $H_i$  and  $\nu_i$  change with the spectral state (cf. Figs. 9, 14 and 15), the other correlations show no such behavior.

A second result of our study was to show that the PDS of Cyg X-1 is dominated by the same two Lorentzian components at all times. We base this conclusion on the fact that we saw no change in the identification of components on our analysis timescale and that the points in Figs. 9 to 15 each describe a continuous distribution. The relation of the peak frequencies of these components follows the pattern seen in both other BHC and NS systems, and we therefore conclude that the physical processes responsible for them cannot be explained by invoking magnetic fields, a solid surface, or an event horizon. A possible model is the RPM of Stella & Vietri (1998, 1999), which describes the hard state data remarkably well, but requires some rather *ad hoc* assumptions to fit the soft state. One possibility is to invoke a change of rotational direction during the state transitions. We find that this scenario alone is insufficient to explain the data, and additional assumptions are still required. Another point that speaks against the rotational reversal model for state transitions is the observed similarity with other sources, some of which are believed to accrete through Roche lobe overflow and thereby not experience any changes in the rotation of the disk.

We also compared the results of transitions from hard to soft, soft to hard and flares for systematic differences. Within our analysis we were unable to differentiate between the three, and we cannot show any way to predict whether such an event will lead to a full source transition or a large flare.

With this study we have shown the importance of looking at the PDS of Cyg X-1 in a broader context covering all the states of the source. To this end we are currently studying the soft state PDS in more detail and adding newly available data. Determining the behavior of the Lorentzian components at higher frequencies will be of great importance for increasing our understanding of the physical processes behind them.

*Acknowledgements.* We wish to thank Juri Poutanen and Andrzej Zdziarski for helpful discussions, and Michiel van der Klis for providing us with the additional data in Fig. 17. We are grateful to an anonymous referee whose comments and suggestions helped improve this paper.

This research has made use of data obtained through the High Energy Astrophysics Science Archive Research Center (HEASARC)

Online Service, provided by NASA/Goddard Space Flight Center. For the ASM lightcurve we used results provided by the ASM/RXTE teams at MIT and at the RXTE SOF and GOF at NASA/GSFC. This work has been partly funded by the Swedish National Space Board.

## References

- Bałucińska-Church, M., Belloni, T., Church, M. J., & Hasinger, G. 1995, *A&A*, 302, L5
- Bardeen, J. M., Press, W. H., & Teukolsky, S. A. 1972, *ApJ*, 178, 347
- Barret, D., Kluzniak, W., Olive, J. F., Paltani, S., & Skinner, G. K. 2004, *ArXiv Astrophysics e-prints*, astro-ph/0412420
- Belloni, T. & Hasinger, G. 1990, *A&A*, 227, L33
- Belloni, T., Mendez, M., van der Klis, M., et al. 1996, *ApJ*, 472, L107
- Belloni, T., van der Klis, M., Lewin, W. H. G., et al. 1997, *A&A*, 322, 857
- Belloni, T., Psaltis, D., & van der Klis, M. 2002, *ApJ*, 572, 392
- Churazov, E., Gilfanov, M., & Revnivtsev, M. 2001, *MNRAS*, 321, 759
- Cui, W., 1999, in *High Energy Processes in Accreting Black Holes*, J. Poutanen and R. Svensson eds., *ASP Conf. Ser.*, 161 (San Francisco:ASP)
- Cui, W., Heindl, W. A., Rothschild, R. E., et al. 1997, *ApJ*, 474, L57
- Cui, W., Zhang, S. N., Focke, W., & Swank, J. H. 1997, *ApJ*, 484, 383
- Cui, W., Feng, Y., & Ertmer, M. 2002, *ApJ*, 564, L77
- di Matteo, T. & Psaltis, D. 1999, *ApJ*, 526, L101
- Ebisawa, K., Ueda, Y., Inoue, H., Tanaka, Y., & White, N. E. 1996, *ApJ*, 467, 419
- Esin, A. A., Narayan, R., Cui, W., Grove, J. E., & Zhang, S. 1998, *ApJ*, 505, 854
- Gierliński, M., Zdziarski, A. A., Done, C., Johnson, W. N., Ebisawa, K., Ueda, Y., Haardt, F., & Philips, B. F. 1997, *MNRAS*, 288, 958
- Gierliński, M., Zdziarski, A. A., Poutanen, J., et al. 1999, *MNRAS*, 309, 496
- Gilfanov, M., Churazov, E., & Revnivtsev, M. 1999, *A&A*, 352, 182
- Jahoda, K., Swank, J. H., Giles, A. B., et al. 1996, in *EUV, X-Ray, and Gamma-Ray Instrumentation for Astronomy VII*, O.H Siegmund ed., *Proc. SPIE*, 2808 (Bellingham, WA: SPIE), 59
- Jernigan, J. G., Klein, R. I., & Arons, J. 2000, *ApJ*, 530, 875
- Kato, S. 1990, *PASJ*, 42, 99
- Kato, S. 2001, *PASJ*, 53, 1
- Klein-Wolt, M. 2004, Ph.D. thesis, Anton Pannekoek Astronomical Institute and Center for High Energy Astrophysics, University of Amsterdam, Amsterdam
- Miyamoto, S., Kitamoto, S., Iga, S., Negoro, H., & Terada, K. 1992, *ApJ*, 391, L21
- Nowak, M. A. 2000, *MNRAS*, 318, 361 (N00)
- Nowak, M. A., Vaughan, B. A., Wilms, J., Dove, J. B., & Begelman, M. C. 1999, *ApJ*, 510, 874
- Okazaki, A. T., Kato, S., & Fukue, J. 1987, *PASJ*, 39, 457
- Pottschmidt, K., Wilms, J., Nowak, M. A., et al. 2000, *A&A*, 357, L17
- Pottschmidt, K., Wilms, J., Nowak, M. A., et al. 2003, *A&A*, 407, 1039 (P03)
- Poutanen, J. 2001, *Advances in Space Research*, 28, 267
- Poutanen, J., Krolik, J. H., & Ryde, F. 1997, *MNRAS*, 292, L21
- Psaltis, D. & Norman, C. 2000, *ArXiv Astrophysics e-prints*, astro-ph/0001391
- Psaltis, D., Belloni, T., & van der Klis, M. 1999, *ApJ*, 520, 262
- Reig, P., Papadakis, I., & Kylafis, N. D. 2002, *A&A*, 383, 202
- Shapiro, S. L. & Lightman, A. P. 1976, *ApJ*, 204, 555
- Shapiro, S. L., Lightman, A. P., & Eardley, D. M. 1976, *ApJ*, 204, 187
- Stella, L. & Vietri, M. 1998, *ApJ*, 492, L59
- Stella, L. & Vietri, M. 1999, *Physical Review Letters*, 82, 17
- Stella, L., Vietri, M., & Morsink, S. M. 1999, *ApJ*, 524, L63 (SVM)
- van der Klis, M. 1995, in *X-Ray Binaries*, W. H. G. Lewin, J. van Paradijs, & E. P. J. van den Heuvel eds., Cambridge Univ. Press, Cambridge
- van der Klis, M. 2004, to appear in *Compact stellar X-ray sources*, Lewin & van der Klis eds., Cambridge University Press, astro-ph/0410551
- van Straaten, S. 2004, Ph.D. thesis, Anton Pannekoek Astronomical Institute and Center for High Energy Astrophysics, University of Amsterdam, Amsterdam
- van Straaten, S., van der Klis, M., di Salvo, T., & Belloni, T. 2002, *ApJ*, 568, 912
- Vikhlinin, A., Churazov, E., & Gilfanov, M. 1994, *A&A*, 287, 73
- Wagoner, R.V. 1999, *Phys. Rep.*, 311, 259p
- Wagoner, R. V., Silbergleit, A. S., & Ortega-Rodríguez, M. 2001, *ApJ*, 559, L25
- Wen, L., Cui, W., & Bradt, H. V. 2001, *ApJ*, 546, L105
- Wijnands, R. 2001, *Advances in Space Research*, 28, 469
- Wijnands, R. & van der Klis, M. 1999, *ApJ*, 514, 939
- Zdziarski, A. A. & Gierliński, M. 2004, *Prog. Theor. Phys. Suppl.*, 155, 99-119
- Zdziarski, A. A., Poutanen, J., Paciesas, W. S., & Wen, L. 2002, *ApJ*, 578, 357
- Zdziarski, A. A. et al. 2004, in preparation
- Zhang, W., Jahoda, K., Swank, J. H., Morgan, E. H., & Giles, A. B. 1995, *ApJ*, 449, 930
- Zhang, W., Morgan, E. H., Jahoda, K., et al. 1996, *ApJ*, 469, L29
- Zhang, S. N., Cui, W., & Chen, W. 1997, *ApJ*, 482, L155